# Single-qubit gates and measurements in the surface acoustic wave quantum computer

S. Furuta,* C. H. W. Barnes, and C. J. L. Doran
*Cavendish Laboratory, Department of Physics, University of Cambridge, Madingley Road, Cambridge CB3 0HE, United Kingdom*
(Received 11 February 2004; revised manuscript received 4 June 2004; published 15 November 2004)

In the surface acoustic wave quantum computer, the spin state of an electron trapped in a moving quantum dot comprises the physical qubit of the scheme. Via detailed analytic and numerical modeling of the qubit dynamics, we discuss the effect of excitations into higher-energy orbital states of the quantum dot that occur when the qubits pass through magnetic fields. We describe how single-qubit quantum operations, such as single-qubit rotations and single-qubit measurements, can be performed using only localized static magnetic fields. The models provide useful parameter regimes to be explored experimentally when the requirements on semiconductor gate fabrication and the nanomagnetics technology are met in the future.

DOI: 10.1103/PhysRevB.70.205320 PACS number(s): 73.21.La, 72.50.+b, 03.67.Lx

## I. INTRODUCTION

Quantum computation promises enormous technological advances in the field of information processing[1–4] and the quest for its realization has attracted many strong contenders in the field of physics and engineering. This paper is concerned with a scheme for quantum computation put forward by Barnes, Shilton and Robinson,[5] which falls into the semiconductor quantum dot category.[6–12] The proposal for quantum computation is based on the results of ongoing experiments that have demonstrated the capture and transport of single electrons in moving quantum, dots.[13–15] The dots are formed when a surface acoustic wave (SAW) travels along the surface of a piezoelectric semiconductor containing a two-dimensional electron gas (2DEG). See Fig. 1 for a schematic diagram of the device. When the SAW is made to pass through a constriction in the form of a quasi-one-dimensional channel (Q1DC), the induced piezoelectric potential drags electrons into and along the Q1DC. In certain parameter regimes the device transports one electron per potential minimum of the SAW.[14] The spin on the trapped electron represents the physical qubit. Quantum computation involves performing qubit operations on the trapped electrons as they move with the speed of the SAW.

Many schemes for quantum computation, such as conventional quantum dots,[6,16] doped silicon,[17] superconducting boxes,[18] and ion traps,[19] involve static qubits. The surface acoustic wave quantum computer, on the other hand, is of the "flying qubit" type, which include linear optics schemes,[20] some ion trap schemes with ion shuttling[21] and schemes based on coherent electron transport in quantum wires.[5,22,23] All these have in common that the carriers of quantum information physically move through space during the computation. Flying qubits have the advantage of being able to distribute information quickly over large distances across the quantum circuit when decoherence times are short and to interface with quantum memory registers at fixed locations. Another advantage of the SAW quantum computation scheme is its ensemble nature. It intrinsically performs time-ensemble computation, in much the same way NMR quantum computation performs molecular-ensemble computations.[24–26] Time-ensemble computation alleviates the demand for single-shot spin measurements and has the advantage of being robust against small random errors.

This paper considers proposals[5] for implementing quantum gates on single SAW qubits using only static magnetic fields generated by surface magnetic gates. Detailed modeling of the gate operation has been accomplished by means of both analytic solutions and numerical simulations of the Pauli equation. We show how electrostatically confined moving electrons behave under the influence of various magnetic fields and discuss the implications for quantum computing with surface acoustic wave electrons.

The physics of the SAW-guided qubit is explained in more detail in Sec. II. In Secs. III and IV, we present results on single-qubit unitary gates and single-qubit readout gates based on the Stern–Gerlach effect. Section V discusses some of the decoherence processes involved in quantum-dot based schemes. Section VI is a summary of the results with parameter regimes of interest for future experiments.

## II. SCHEME FOR QUANTUM COMPUTATION

We begin by summarizing the quantum computation scheme proposed by Barnes, Shilton and Robinson.[5] Figure 1 shows a schematic diagram of the experimental setup originally designed to demonstrate quantized currents in semiconductors.[13–15] A NiCr/Al interdigitated transducer is patterned on a GaAs/AlGaAs heterostructure. A narrow depleted Q1DC splits the 2DEG into two regions, the source and drain. When a high frequency AC signal is applied to the transducer, a SAW propagates through the 2DEG, producing

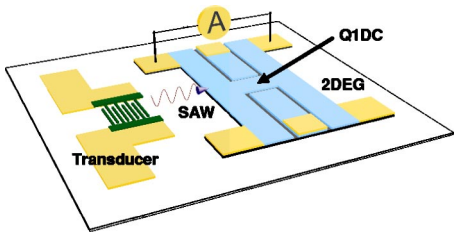


FIG. 1. (Color online) Schematic diagram of an experimental device for producing quantized acoustoelectric currents through a narrow Q1DC constriction.

 

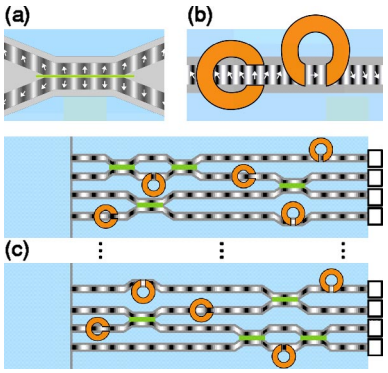


FIG. 2. (Color online) Schematic diagram of a quantum gate network in a SAW quantum computer: (a) two-qubit tunneling gates; (b) one-qubit magnetic gates (in various orientations); (c) gate network for quantum computation with SAW electron spins. Gray lines running horizontally represent Q1DCs; blackened regions indicate the SAW minima where the qubits reside; arrows represent spin polarization; rings represent magnetic surface gates; white squares represent readout gates.

a periodic piezoelectric potential across the 2DEG. The potential drags electrons in the source region through the narrow Q1DC constriction into the drain. It has been shown experimentally that over a range of SAW power and gate voltages, the current passing through the Q1DC is quantized in units of $ef$, where $e$ is the electronic charge and $f$ is the frequency of the SAW.[13–15] The smallest quantized current observed corresponds to the transport of a single electron in each SAW minimum. Typically, the SAW in GaAs moves at 2700 $ms^{-1}$ at a frequency of around 2.7 GHz, with an applied power of 3–7 dBm.[14] These parameters produce currents in the range of nanoamps.

Given the ability to trap single electrons in the SAW minima, the scheme for quantum computation is as follows. It is possible for an array of $N$ Q1DCs in parallel to capture $N$ qubits in every $M$th minimum, with a single electron in each Q1DC, producing a qubit register along the SAW wavefront. $M$ can be chosen sufficiently large to ensure that the Coulomb interaction between successive qubit registers do not interfere with each separate computation. The qubits move with the minima of the SAW, passing through a sequence of static one- and two-qubit gates before arriving at an array of spin readout devices. Single-qubit gates may be operated by nanoscale electromagnetic fields. Where two-qubit gates are needed, neighboring Q1DCs are allowed into a tunnel contact controlled by a potential on a surface gate.[5] The use of the Coulomb coupling between neighboring Q1DCs is a common tool in spintronics which can be used to generate entangled states in dual-rail qubit representations.[27,28] Figure 2 illustrates the network of Q1DCs and qubit gates envisaged for performing a particular quantum computation.

The SAW-trapped electron is well confined in all three spatial directions. In this paper we define Cartesian coordinates such that the SAW propagates along the $x$ axis with the $z$ axis normal to the 2DEG. The 2DEG is produced by a band-energy mismatch at the GaAs/AlGaAs interface which gives rise to a confining potential in the $z$ direction. The energy level spacings in the 2DEG well are on the order of 50–100 meV.[29] Further confinement in the $y$ direction is provided by an extended Q1DC, etched into the surface so as to avoid screening the SAW-induced potential with metallic surface gates.[30] Finally, the confinement in the $x$ direction is due to the SAW potential minimum which is approximately sinusoidal. The SAW amplitude is typically 40 meV,[31] which is sufficiently large to prevent qubits being lost via tunneling into neighboring SAW minima.

There are two important aspects of the SAW quantum computation scheme that distinguish it from other similar quantum dot schemes. First, the scheme provides repetitions of the same quantum computation with each passing of a single wavefront of the SAW. Therefore, a statistical time-ensemble of identical computations can be read out at the end of the Q1DCs as a measurable current, alleviating the need for single-electron measurements. Two sources of noise in the measured current may be estimated as follows: The shot noise is largely determined by how well the current is quantized to $I=ef_{\mathrm{SAW}}$ and precisions of $<0.1\%$ can be experimentally achieved.[32] Johnson noise arises from the resistance of the ohmic contacts and the 2DEG which are on the order of 100–1000Ω. At temperatures of 1 K they produce a rms voltage noise spectral density on the order of $10^{-10}$ $V/\sqrt{\mathrm{Hz}}$ at most. This cannot drive a current noise through the SAW device since its effective intrinsic impedance of 10 MΩ is comparatively very large. See experimental papers in Refs. 13–15, 32, and 33 for more detailed discussions. The second key aspect of the scheme is the static nature of the gate components of the quantum circuit. This alleviates the need for strong, targeted and carefully timed electromagnetic pulses that can be difficult and expensive to implement. The requirement of such expensive control resources often limit the scalability of most quantum computing implementations.

It would certainly be convenient, though not essential, to have a means of preparing a pure fiducial qubit state. In NMR quantum computing, operations are carried out on ensembles of replica qubits which remain close to a highly mixed state of thermal equilibrium. Nevertheless, a successful readout of the computation is obtained because the sum over many identical computations provides a measurable signal. Similarly in the SAW quantum computing scheme, states close to the maximally mixed state are still useful because of the time-ensemble nature of the scheme. However, in contrast to NMR schemes, it is in principle possible to read out single electrons in the SAW scheme. We will therefore begin with nonensemble quantum computation in mind and only later exploit the advantages of ensemble computation to deal with noise. Of course, the more pure the qubit states remain, the faster the computation will converge to the result. For these reasons, we describe in this paper two simple methods for preparing pure fiducial qubit states.

In the original proposal for the SAW quantum computer,[5] it was noted that the application of an external magnetic field of about 1 T will influence which spin states of electrons are favored in the capture process.[31] This polarized capture process can be summarized as follows. The SAW is strongly screened in the bulk 2DEG until it is raised above the Fermi energy and the quantum dot begins to form. When the

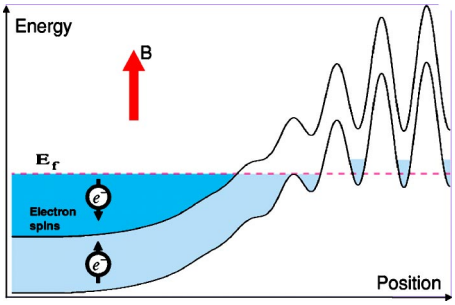


FIG. 3. (Color online) Energy diagram showing polarized electron capture by means of Zeeman band splitting in the presence of a uniform magnetic field: Arrows on electrons indicate spin polarizations; $E_f$ is the Fermi energy. The SAW is strongly screened in the bulk 2DEG below the Fermi energy. As the SAW enters the Q1DC constriction, the confining potential begins to form. The probability of capturing spin-down is small at the point the minority spin-type dot forms (upper curve). In contrast, the probability of capturing spin-up electrons is high when the majority spin-type dot forms (lower curve).

higher-energy minority quantum dot forms for the higher-energy subband of polarized electrons, the probability of capturing minority electrons is small (see Fig. 3), while the probability of capturing electrons from the lower-energy subband is large. Once a cloud of approximately polarized electrons is captured, the exchange interaction will generally entangle electrons in the same dot together, so that the subsequent loss of electrons into the Fermi sea will lead to a decoherent process that could relax the remaining electrons into the low-energy polarized state. A more detailed multiparticle analysis will be needed to determine the final state of the remaining single electron, but the combination of the above two processes is likely to lead to a high level of polarization.

The above method is conceptually simple and would be easy to implement in the laboratory. However, the macroscopic magnetic field required in the capture region may need to be shielded from the rest of the device where the quantum computation is to be carried out, and this may present a nontrivial problem. If we chose to drive spin flips using microwave pulses, then the macroscopic field is in fact required across the whole device. However, the problem with using microwaves is their relatively long wavelength, which tends to affect every part the computation. Alternatively, we may use local, static magnetic fields to initialize, rotate and read out single qubits without a global magnetic field. In Sec. IV, it will be demonstrated that spin-polarized electrons can be prepared and measured using a gate driven by the Stern–Gerlach effect. First we turn to the implementation of single qubit rotations using local static magnetic gates.

## III. SINGLE-QUBIT UNITARY GATES

Single-qubit unitary operations may be carried out, in principle, by allowing the trapped single electrons to pass through regions of uniform magnetic field. If there is no spin-orbit coupling effect, the spin state of the qubit will evolve according to the Zeeman term in the Hamiltonian: $\frac{1}{2}g\mu_B\mathbf{B}\cdot\boldsymbol{\sigma}\psi$, where $\mathbf{B}$ is the magnetic field, $\boldsymbol{\sigma}$ is the vector form of the three Pauli operators and $\psi=(\alpha,\beta)$ is a spinor. The Bloch vector $n=(-2\,\mathrm{Im}[\alpha\beta^*],2\,\mathrm{Re}[\alpha\beta^*],|\alpha|^2-|\beta|^2)$ precesses about the direction of the magnetic field with angular frequency $g\mu_B|B|/\hbar$. A local static magnet may be produced by a magnetic force microscope or by evaporative deposition of a ferromagnetic material such as Cobalt, or a permalloy such as NiFe. Inevitably, different samples will produce different strengths of magnetic field. But there are methods to vary the strength and pattern of the field once the sample has been fabricated. It has been demonstrated that ferromagnetic properties of thin-film 3D transition metals can be modified via ion irradiation.[34] Another method would be to use oxidation techniques with the atomic force microscope.[35–37] Only two independent directions of the B-field are necessary to produce an arbitrary single-qubit manipulation and we will choose these to be perpendicular to the direction of the SAW, one aligned with and the other perpendicular to the 2DEG.

For idealized qubits with no spatial degree of freedom, the above model for single-qubit rotations is complete. However, the trapped electron is a charged particle with a spatial distribution within the dot. The fields couple to both the spatial and spin degrees of freedom, causing the electron to experience the Lorentz force as well as spin-precession. It is therefore clear that one cannot increase magnetic fields arbitrarily, since the Lorentz force will upset the confinement properties of the electron. Nor can the direction of the field be chosen arbitrarily without consequences for the robustness of the gate. To address these concerns, we analyze the behavior of the full spinor field, $\psi_\sigma(\mathbf{x},t)$, under the action of gates operated by static magnets.

### A. Pauli Hamiltonian with uniform magnetic fields

Assuming a uniform magnetic field in the lab frame, we solve the Pauli equation for the spin field from which the probability density field and the Bloch vector field can be obtained.

The qubit is trapped in a net electrostatic potential with contributions from the Q1DC split gates, the 2DEG confining potential and the SAW piezoelectric potential. The parameter regimes we consider allow us to neglect motion out of the 2DEG plane.[67] The net confining potential in the $xy$ plane is modeled by[31]

$$V = V_{\mathrm{Q1DC}} + V_{\mathrm{SAW}} = V_0\frac{y^2}{2w^2} + A\{1-\cos[2\pi(x/\lambda - ft)]\}. \tag{1}$$

The Q1DC split gate voltages are such that typically $V_0 \sim 2800$ meV. The width of the Q1DC $w$ is typically between 1 and 2 $\mu$m. The amplitude of the SAW is $A \sim 40$ meV with wavelength $\lambda \sim 1$ $\mu$m and frequency $f \sim 2.7$ GHz.

The appropriate nonrelativistic equation for the two-component spinor field is the Schrödinger equation with a Pauli Hamiltonian. For an electron moving in an arbitrary vector potential $A$ and potential energy $V$, the Pauli Hamiltonian reads

$$H = \frac{1}{2m^*}(\hat{p}^2 + e(\hat{p}\cdot A) + 2eA\cdot\hat{p} + e^2A^2) + \frac{1}{2}g\mu_B\sigma\cdot B + V, \tag{2}$$

where $e>0$ is the electronic charge, $g\simeq 0.44$ is the Landé g-factor and $m^*\simeq 0.067m_e$ is the effective mass in GaAs. By simulating in the plane of the 2DEG we simplify to a 2+1 dimensional model, with variables $(x,y,t)$. If the particle were chargeless but with an anomalous magnetic moment, terms in $H$ that explicitly involve $e$ can be dropped. In such a case, there is no Lorentz force acting on the particle, the Schrödinger equation simplifies significantly and there would be no need to concern ourselves with the spatial behavior of the qubit.

Before proceeding further, it is convenient to transform into the rest frame of the electron moving with the SAW speed $v$. We may use simple Galilean transformations $x'=x-vt$, $y'=y$, $t'=t$, since the SAW velocity is nonrelativistic. The potentials in the electron rest frame become, in the harmonic oscillator approximation,

$$A(x',t') = -\beta(x'+vt'), \tag{3}$$

$$V(x',y') = V_0\frac{y'^2}{2w^2} + A\left[1-\cos\left(\frac{2\pi x'}{\lambda}\right)\right] \tag{4}$$

$$\simeq \frac{V_0}{2w^2}y'^2 + \frac{A}{2}k^2x'^2, \tag{5}$$

with $k=2\pi/\lambda$. A further convenience is to use a system of natural units such that $\hbar$, $m^*$, $v$, $e$ are unity. The units of length, time and energy become $\hbar/m^*v=0.640$ $\mu$m, $\hbar/m^*v^2=0.237$ ns and $m^*v^2=2.78$ $\mu$eV, respectively. The natural unit of magnetic field is 1.61mT. Parameters can now be assigned dimensionless values with respect to the above units. In the electron rest frame,

$$-\frac{1}{2}\nabla^2\psi - i\left[A\cdot\nabla + \frac{1}{2}(\nabla\cdot A)\right]\psi + \frac{1}{2}A^2\psi + \frac{1}{2}g\mu_B\sigma\cdot B\psi + V\psi = i\frac{\partial}{\partial t}\psi, \tag{6}$$

where the primes will subsequently be dropped from the coordinates. We will further simplify the Hamiltonian by adopting the Coulomb gauge $\nabla\cdot A=0$.

### B. Qubit rotation: Uniform transverse magnetic field

For a magnetic field in the $y$ direction in the plane of the 2DEG and transverse to the Q1DC, we model the magnetic field in the region of the single-qubit gate with a vector potential of the form

$$A_z(x) = -\beta x, \tag{7}$$

with $A_x=A_y=0$. Clearly this does not vanish at infinity, but we only consider interactions over regions of finite extent. This potential generates a uniform magnetic field of strength $\beta$ in the $y$ direction. With this potential Eq. (6) becomes

$$-\frac{1}{2}\nabla^2\psi + \frac{1}{2}\beta^2(x+t)^2\psi + \frac{1}{2}g\mu_B\beta\sigma_y\psi + V\psi = i\frac{\partial}{\partial t}\psi, \tag{8}$$

in which the potential $V$ is given by (5). An effective potential $V+A^2/2$ can be identified, which resembles a harmonic oscillator but is time-dependent. Anticipating an analytic solution by separation of variables we apply the ansatz

$$\psi_\pm(x,y,t) = \chi(x,t)\phi_n(y)e^{-iE_nt}|s_y\rangle e^{-is_y\Delta Et/2}, \tag{9}$$

where $\phi_n$ are the harmonic oscillator eigenstates with energies $E_n=\omega_y(n+\frac{1}{2})$, and $|s_y\rangle$ are the eigenstates of $\sigma_y$ with eigenvalues $s_y=\pm 1$. We have introduced the oscillator frequency $\omega_y=\sqrt{V_0}/w$ and the Zeeman energy gap $\Delta E=g\mu_B\beta$. The energy eigenstates in the $y$ direction are exactly the harmonic oscillator modes. The wavefunction in the $x$ direction is time-dependent and it is the solution of $\chi(x,t)$ to which we now turn. On substituting (9) into (8), we obtain a PDE for $\chi(x,t)$:

$$-\tfrac{1}{2}\partial_x^2\chi + \left[\tfrac{1}{2}(c_0+c_1)x^2 + c_1xt\right]\chi = i\partial_t\chi, \tag{10}$$

with $c_0=Ak^2$ and $c_1=\beta^2$. Terms which depend only on $t$ have been dropped, as they merely contribute global, time-dependent phases that do not affect the dynamics. A Gaussian solution of (10) can be found with a further ansatz:

$$\chi(x,t) = \exp[f_1(t)x^2 + f_2(t)x + f_3(t)]. \tag{11}$$

This system of time-dependent functions can be determined self-consistently, assuming a Gaussian groundstate of the SAW dot with standard width $s$ at $t=0$. The resulting expressions for $f_1$, $f_2$, $f_3$ are complicated, but by noting a few general properties of the solution we can understand all the important features of the dynamics. $f_3(t)$ takes account of the normalization but is otherwise of no more interest. $f_1(t)$ and $f_2(t)$ together describe a groundstate Gaussian wavefunction evolving in the time-dependent vector potential. The solution is particularly simple in that it remains Gaussian throughout, so we will only need to keep track of the position of the central peak $\mu$ and the width (standard deviation) $\delta$ of the probability distribution $|\chi(x,t)|^2$:

$$\mu(t) = -\frac{1}{2}\frac{\mathrm{Re}[f_2(t)]}{\mathrm{Re}[f_1(t)]}, \tag{12}$$

$$\delta(t) = \tfrac{1}{2}\sqrt{-\mathrm{Re}[f_1(t)]}. \tag{13}$$

The typical energy scales for the SAW electron encountered in experiment puts the system in the regime where $s\ll 1$ and $c_1\ll c_0$. Expanding $f_1$ and $f_2$ to first order in $s$ and $c_1/c_0$, we obtain the asymptotic behavior for the position of the peak:

$$\mu(t) \to \frac{-c_0}{c_0+c_1}t. \tag{14}$$

From this result we see that the magnetic field introduces a constant drift velocity of the peak in the $-x$ direction. On exiting the interaction region, the peak will be off-center with respect to the SAW dot and the probability distribution will subsequently oscillate in the $x$ direction, perhaps exciting higher-energy orbital states of the dot. If the charge dis-

tribution is pulled too far off-center, it is likely to escape the SAW quantum dot. We could ask how long the electron can remain in the field before it is dragged a distance λ away from the center of the dot in the $x$ direction:

$$T_{\max} \simeq \frac{c_0 + c_1}{2c_0}\lambda. \tag{15}$$

When this is compared with the time required for the Bloch vector to rotate by some appreciable angle such as a $\pi$ rotation, we obtain the ratio

$$T_{\max}/T_{\pi} = g\mu_B \frac{\beta}{k}\left(\frac{Ak^2 + \beta^2}{Ak^2}\right), \tag{16}$$

which is about 10 for a 1 T field. Therefore, while it is possible that higher orbital states are excited as a consequence of the interaction, there is little danger of the electron escaping the SAW quantum dot during the operation of the gate. We now turn to the behavior of $\delta(t)$, the width of the Gaussian wavefunction, which in the limit $c_1 \ll c_0$ oscillates according to the simple expression

$$\delta(t) = \sqrt{\frac{\sqrt{c_0}}{2(c_0 + c_1)}}\left[1 + \frac{c_1}{c_0}\cos^2(\sqrt{c_0 + c_1}t)\right]^{1/2}, \tag{17}$$

with $c_0 = Ak^2$ and $c_1 = \beta^2$. The frequency of the oscillation increases with the energy of the dot and is typically much faster than the Zeeman spin precession frequency, i.e., rate of precession of the qubit Bloch vector. These results are plotted for a specific case in Fig. 4. The top two plots show the evolution of $\mu$ and $\delta$. As the Bloch vector rotates about the field along the $y$-axis, the Gaussian translates in the $x$ direction with a rapidly oscillating width. The bottom plot of Fig. 4 shows probability amplitudes of excitation into higher-energy simple harmonic oscillator (SHO) modes in the $x$ direction of the quantum dot.

Our conclusions are as follows. In addition to rotating the Bloch vector as required, the gate has the effect of displacing the center of the Gaussian wavefunction which will increase the energy of the bound state by an amount depending on both the gate time and the field strength. Higher-energy orbital states are likely to be excited, which could lead to decoherence via spin-orbit couplings or dipole coupling to phonons and photons. According to Fig. 4, the electron is almost completely out of the groundstate after a $\pi/2$ rotation of the Bloch vector. In the extreme case after many spin precessions, the qubit will leave the SAW quantum dot. However, for quantum computations the gate time need only be long enough to conduct a single orbit of the Bloch sphere, in which case the excitation into higher orbital states is negligible. These observations reveal some important features of the gate operation that are not revealed by an idealized spin-only model of the qubit.

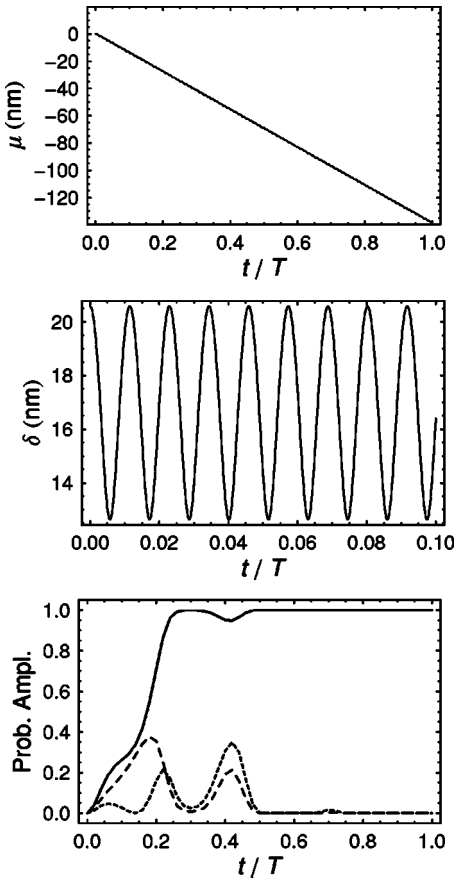


FIG. 4. Gaussian evolution of the probability distribution $|\chi(x,t)|^2$ in a constant magnetic field $B_y$. The top plot shows peak position $\mu$ and the middle plot shows the width $\delta$. The bottom plot shows the probability amplitudes $|C_n|^2$ of the $n$th SHO mode in the $x$ direction: $|C_1|^2$ (long dash), $|C_2|^2$ (short dash). The plot also shows $1-|C_0|^2$ (solid). Typical values for the SAW dot are taken: $A=40$ meV; $\lambda=1.0$ $\mu$m; magnetic field of 1 T. $T=\pi/g\mu_B\beta \approx 0.08$ ns is the time taken for a $\pi$ rotation of the Bloch vector about the $y$-axis. The initial Gaussian wavefunction was taken to be the SAW quantum dot groundstate ($C_0=1$). In the limit $c_1/c_0 \ll 1$ (weak field), $\mu(t)$ moves approximately linearly and $\delta(t)$ undergoes bounded oscillations about $\delta(0)=s/\sqrt{2}$.

### C. Qubit rotation: Uniform perpendicular magnetic field

To move the qubit state to an arbitrary point on the Bloch sphere a second axis of rotation on the Bloch sphere is needed, and to this end we consider a gate implemented by a uniform magnetic field in the $z$ direction. This will not be just a trivial extension of the preceding analysis, since the 3D rotation symmetry is broken by the motion of the SAW in the $x$ direction. In practice, the $y$ magnetic field may be easier to fabricate than the $z$ magnetic field, since the latter passes perpendicularly through the 2DEG structure. It could feasibly be produced by layering oppositely aligned thin-film magnets just beneath and just above the 2DEG, or by applying a global $z$ magnetic field which is shielded in regions where it is not needed.

A vector potential generating the uniform $B_z$ magnetic field is

$$A_x(y) = -\beta y, \tag{18}$$

with $A_y = A_z = 0$. It should be noted that although the field is uniform and static in the laboratory frame, the electron sees a moving uniform field. In the electron rest frame, $A_x$ is time-independent and $z$-independent, allowing a Hamiltonian in $x$

and $y$ only. The chosen gauge facilitates numerical simulations which follow shortly. An effective scalar potential that is quadratic in $y$ arises from the $A^2$ term in the Hamiltonian (6). It is interesting to compare the strength of this confining potential with the Q1DC potential, which is also approximately quadratic in $y$:

$$\frac{\text{Energy of A}^2\text{ term}}{\text{Energy of Q1DC term}} = \frac{\beta^2}{V_0/w^2}. \tag{19}$$

With magnetic fields of order 1 T and typical Q1DC energies, this ratio is of order unity. This means that for the parameter values being considered the effective scalar potential arising form the $A^2$ term is comparable to the Q1DC confinement potential. A stronger field would start to significantly deform the shape of the dot. This will not be a problem as long as the evolution has occurred adiabatically during the deformation. However, as we shall discuss in a moment, the probability of excitation into higher orbital states due to the $B_z$ field is not negligible.

The other interesting term in the Hamiltonian is the asymmetric coupling $-i\beta y\partial_x$ between the $x$ and $y$ variables. This is expected to introduce rotational behavior, as we would intuitively anticipate some form of Landau orbital motion due to the Lorentz force.

A Crank–Nicholson[38] finite difference algorithm (alternating direction method) was used to simulate the operation of the gate. We started with an initial Gaussian groundstate of the dot with spin state $|\uparrow_x\rangle$ and subjected it to 1 T of magnetic field for a duration of $T_{\pi/2}=\pi/2g\mu_B\beta$, which is the gate time required for a $\pi/2$ rotation of the Bloch vector about the $z$ axis. The evolution of the Bloch vector is simple due to the uniformity of the magnetic field: $n_x(t)=\cos(g\mu_B\beta t)$, $n_y(t)=\sin(g\mu_B\beta t)$, and $n_z(t)=0$ All other parameters were assigned those values given just after Eq. (1). The result of the simulation is shown in Fig. 5, which shows time-shots of the probability distribution in the 2DEG ($xy$) plane. Losing its initial elliptic contours, the distribution develops two lobes which rotate about its midpoint. The density at the center increases due to the spatial squeezing from the $A^2$ term in the Hamiltonian. This clearly shows excitation into higher-energy orbital states.

Using perturbation theory to second order in the strength of the field $\beta$, with harmonic oscillator modes as the basis, we found the following facts: (*i*) To second order of perturbation theory, only the second excited state with SHO quantum numbers $n_x=n_y=1$ becomes populated. (*ii*) The probability ratio with respect to the groundstate is

$$\left|\frac{C_{11}}{C_{00}}\right|^2 = \beta^2\frac{\omega_x \sin^2[t(\omega_x+\omega_y)/2]}{\omega_y(\omega_x+\omega_y)^2}, \tag{20}$$

where $\omega_x$ and $\omega_y$ are frequencies arising from the harmonic oscillator approximation. (*iii*) The amplitude of the ratio approaches unity when the field approaches 1 T. (*iv*) The ratio of the spin precession frequency to the frequency of the $|C_{11}|$ oscillation is about $1.6\times10^{-5}$ for typical SAW parameters [see just after Eq. (1)].

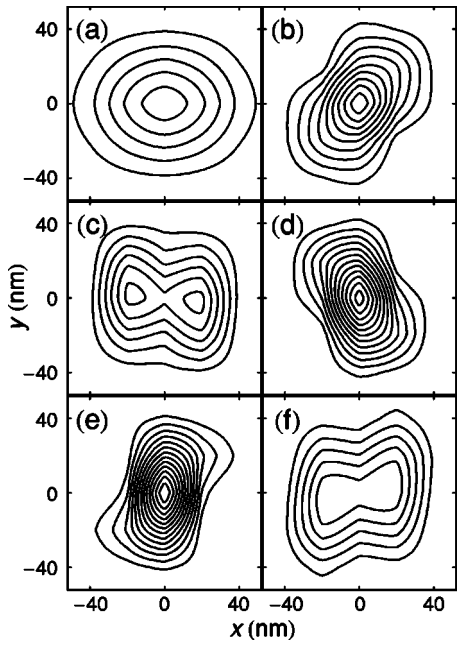


FIG. 5. Contour plots of electron probability density during the operation of a qubit rotation gate. This is a numerical simulation in the $xy$ (2DEG) plane of a SAW electron undergoing a $\pi/2$ rotation gate about the $z$ axis, under a uniform magnetic field $B_z$ of strength 1 *T*. Snap-shots are shown at the following times (ps): (a) 0, (b) 2.89, (c) 11.6, (d) 20.3, (e) 28.9, (f) 37.6. The initial probability distribution is a Gaussian groundstate with standard widths $\sigma_x=26.0$ and $\sigma_y=20.6$. The probability density rotates about the $z$ axis under the influence of the Lorentz force acting in the $xy$ plane. Moreover, an effective scalar potential contributed by the $A^2$ term in the Hamiltonian is quadratic in $y$, which spatially squeezes the initial Gaussian distribution into the center of the dot.

The above model is useful in assessing the robustness of the qubit and its susceptibility to decoherence due to orbital motion. Population into this excited state is a problem for decoherence, since the oscillating charge in the dot couples via dipole interactions to phonons and other charges outside the dot. However, provided we have sufficient control of the gate time, we can use (20) to make the electron exit from the gate in its groundstate. Otherwise, a gate driven by radiofrequency pulses in the presence of a global magnetic field could provide an alternative means to implement spin rotations about the $z$ axis.

## IV. SINGLE-QUBIT INITIALIZATION AND MEASUREMENTS

In addition to single-qubit rotation gates, we require the ability to initialize and measure qubits at the beginning and end of the computation. Spin-polarized electrons can be obtained from injection through a ferromagnetic contact.[39,40] There is also a method to polarize spin using nondispersive phases (Aharonov-Bohm and Rashba) without the need for ferromagnetic contacts.[41] In the field of quantum computing, a well-known method for achieving readout of solid state spin qubits is to convert spin information into charge information[6] and subsequently use single-electron transistors

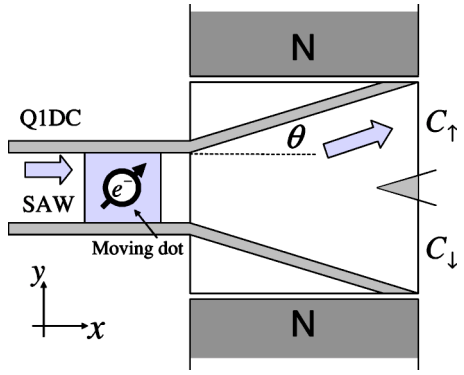


FIG. 6. Schematic diagram of the spin readout/polarizing device based on the Stern–Gerlach effect: SAW propagates from left to right transporting a single electron in a moving quantum dot. Q1DC relaxes with a gradient $\tan(\theta)$ to partially delocalize the particle during the gate operation; $C_\uparrow(C_\downarrow)$ labels the Q1DC receiving electron flux in the spin up(down) state of the $\sigma_y$ operator. Magnets (of any geometry and polarity) need to produce a localized, inhomogeneous distribution of magnetic field.

or point contacts to detect charge displacements or Rabi oscillations.[42,43] However, recent theoretical results by Stace and Barrett[44] argue the absence of coherent oscillations in a continuously measured current noise, contrary to previous results and assumptions,[45,46] and therefore raise concerns about the measurability of charge oscillations in similar scenarios. In any case, it is difficult to apply these methods to qubits in moving quantum dots. We therefore turn towards a quite different approach, one which enables the initialization and readout of SAW electron spin qubits solely with the aid of nanomagnets and ohmic contacts.[5]

The readout gate we consider is based on the Stern–Gerlach effect.[47–49] In the 1920s Bohr and Pauli asserted that a Stern–Gerlach measurement on free electrons was impossible,[50,51] using arguments which combined the concept of classical trajectories and the uncertainty principle. This subsequently led physicists to analyze single-electron Stern–Gerlach measurements within increasingly more rigorous quantum settings, ultimately ending the debate by showing that the measurement can indeed be done, albeit with certain caveats.[52–54] Thus Stern–Gerlach measurements on *free* electrons have been extensively investigated, but little attention has been given to such measurements on confined electrons.[55] An interesting semiclassical analysis of a Stern–Gerlach type experiment with conduction electrons has been reported,[56] in which the authors justifiably neglect the Lorentz force effects. In contrast, we analyze a single-electron Stern–Gerlach device, providing a full quantum mechanical treatment and including all Lorentz force effects.

The electron confinement to low dimensions allows us to guide the electron through the magnetic field in ways that enhance the spin measurement and suppress the deleterious effects of delocalization and the Lorentz force. Surface magnets can be arranged in such a way as to produce a local magnetic field inhomogeneity. For example, two north poles placed on either side of the Q1DC will produce a region of intense magnetic field gradient in between (see Fig. 6). Via the Zeeman interaction term $\propto\sigma\cdot B$ in the Pauli Hamiltonian, the field inhomogeneity has the effect of correlating the spatial location of a wavepacket to its spin state.[57] In most situations it is necessary to continue confining the qubit during the operation of the gate, because the spreading time[68] for a free Gaussian wavefunction is comparatively short—on the order of 1 ns. But the gate must cause a wavepacket splitting in order for the spin states to be resolved, hence the Q1DC must relax to allow for motion in the $y$ direction. This is achieved by patterning the Q1DC in a funnel shape, with an opening angle $\theta$ (see Fig. 6), such that in the electron rest frame the potential looks like

$$V_{\mathrm{Q1DC}} = V_0 y^2/2[w + \tan(\theta)u(t)t]^2, \tag{21}$$

where $u(t)$ is the step function: $u(t<0)=0$ and $u(t\geqslant 0)=1$. A negatively biased surface gate placed on the $x$ axis can be used to guide the electron into the channels. If necessary, both the position of the electrode and the opening angle $\theta$ could be optimized for a particular sample device under low-temperature and high-vacuum conditions by erasable electrostatic lithography.[58] We will study the quality of the readout obtained from the gate for two different magnetic field configurations, both sufficiently simple so as to be realizable in the near future: the linearly inhomogeneous field and the 2D dipole field.

### A. Stern–Gerlach gate using a linearly inhomogeneous field

In the first model we will analyze a simple, unidirectional and linearly inhomogeneous field pointing in the $y$ direction:

$$B_y = -\beta y, \tag{22}$$

with $B_x=B_z=0$. A wedge-shaped single domain surface magnet of appropriate dimensions can produce an inhomogeneous magnetic field of this form near its center of symmetry. A vector potential for this field is $A_x=-\beta yz$, with $A_y=A_z=0$. This field exerts a spin-dependent force in the $y$ direction and it is the simplest field that induces the Stern–Gerlach effect. Although a $z$ dependence enters into the vector potential, by considering motion only in the $z=0$ 2DEG plane we may avoid contributions from terms involving $A$ in the Hamiltonian, as well as the $z$ component of magnetic field. The absence of $x$ in the potential immediately allows us to write down harmonic oscillator modes for the $x$ dependence. The remaining $(y,t)$ dependent part obeys

$$-\tfrac{1}{2}\nabla^2\psi(y,t) - \tfrac{1}{2}g\mu_{\mathrm{B}}\beta s_y y\psi(y,t) + V_{\mathrm{Q1DC}}(y,t)\psi(y,t) = i\partial_t\psi(y,t), \tag{23}$$

where $s_y$ is the eigenvalue $\pm 1$ of the spinor $|s_y\rangle$, and $V_{\mathrm{Q1DC}}$ is given by (21). The initial state is again the Gaussian ground state of the Q1DC. A solution to (23) is obtained by a time-dependent Gaussian ansatz (11)

$$\psi(y,t) = \exp[f_1(t)y^2 + f_2(t)y + f_3(t)]. \tag{24}$$

In a similar way as before, we solve the system of coupled ordinary differential equations and derive the time dependence of the standard deviation $\delta(t)$ and the position $\mu(t)$ of the probability distribution.

Let $c_0=V_0/w^2$ and $c_1=g\mu_{\mathrm{B}}\beta s_y$. The width of the initial Gaussian groundstate wavefunction is $s=c_0^{-1/4}$. The behavior

of the Gaussian solution is then characterized by its width $\delta$ and peak position $\mu$,

$$\delta(\tau)^2 = \frac{\tau}{2\gamma\sqrt{c_0}}[-4c_0 + \alpha^2\cosh(\sqrt{\gamma}\ln(\tau)/\alpha) - \alpha\sqrt{\gamma}\sinh(\sqrt{\gamma}\ln(\tau)/\alpha)], \tag{25}$$

$$\mu(\tau) = \frac{\sqrt{\tau}c_1}{2(2\alpha^2 + c_0)}\left[\tau^{3/2} - \cosh(\sqrt{\gamma}\ln(\tau)/\alpha) - \frac{3\alpha}{\sqrt{\gamma}}\sinh(\sqrt{\gamma}\ln(\tau)/\alpha)\right], \tag{26}$$

where we have introduced ancillary variables $\alpha=\tan(\theta)/w$, $\gamma=\alpha^2-4c_0$ and $\tau=1+\alpha t$. The parameter $\gamma$ is useful in determining when the trigonometric functions become oscillatory. If the angle $\theta$ is critical such that $\tan(\theta)=2\sqrt{V_0}$, then $\gamma=0$ and the width has an especially simple behavior:

$$\delta(t)^2 = \frac{\tau}{\alpha}\left[1 - \ln\tau + \frac{1}{2}(\ln\tau)^2\right]. \tag{27}$$

For a weak magnetic field such that $c_0 \gg c_1 \gg \alpha$,

$$\delta(\tau) = \sqrt{\frac{\tau}{2\sqrt{c_0}}} = \delta(0)\sqrt{1 + \tan(\theta)\frac{t}{w}}, \tag{28}$$

$$\mu(\tau) = \frac{c_1}{2c_0}\left[\tau^2 - \sqrt{\tau}\cos\left(\frac{\sqrt{c_0}}{\alpha}\ln\tau\right)\right]. \tag{29}$$

The width increases as $\sim\sqrt{t}$ and the position moves as $\sim t^2$ as expected. We may compare $\delta(t)$ with the dispersion of a Gaussian in free space

$$\delta(t) = \sqrt{\delta(0)^2 + \frac{t^2}{4\delta(0)^2}}, \tag{30}$$

which is linear in $t$ at large times. The broadening of the width is suppressed due to the confinement potentials. The effect of the Stern–Gerlach gate can be pictured as follows. Consider a qubit in the state $|\uparrow_y\rangle$ entering the gate. The Q1DC broadens as the qubit enters the field, allowing the Stern–Gerlach effect to produce a spin-dependent shift in the center of mass towards the channel $C_\uparrow$. However, the initial localized distribution will delocalize due to the Q1DC broadening, allowing a small current to be detected in the wrong channel $C_\downarrow$. Thus this gate is a spin polarizing filter with some intrinsic error rate which is independent of decoherence effects, shot noise and Johnson noise. It remains for us to judge how well it performs, and to this end we introduce a fidelity measure of the gate.

### B. Fidelity of the Stern–Gerlach gate with linearly inhomogeneous field

As an input to the Stern–Gerlach gate, we consider a density matrix of the form

$$\rho(y,y') = g(y)g(y')^* \otimes \sigma, \tag{31}$$

where $g(y)$ is the Gaussian groundstate of the dot and $\sigma$ is the initial spin density matrix. In the inhomogeneous field the spatial degrees of freedom couple to the spin degrees of freedom, leading to

$$\rho(y,y',t) = \sum_{s,s'=\uparrow,\downarrow} g_s(y,t)g_{s'}(y',t)^* \sigma_{ss'}|s\rangle\langle s'|. \tag{32}$$

After a gate time $t$, we post-select the state in, say, the $C_\uparrow$ channel and renormalize:

$$\tilde{\rho}(y,y',t) = \frac{1}{N(t)}\sum_{s,s'}\sigma_{ss'}|s\rangle\langle s'|\int dz dz'\, E_\uparrow(y,z)g_s(z,t) \times g_{s'}(z',t)^* E_\uparrow(z',y'). \tag{33}$$

The probability yield in the channel is the normalization $N(t)$ of the postselected state. The simplest projection kernel projecting into the support of $C_\uparrow$ is $E_\uparrow(y,y')=\delta(y-y')u(y)$, where $u(y)$ is the step-function defined in (21). We finally define our fidelity as

$$F_\uparrow = \int dy\, \langle\uparrow|\tilde{\rho}(y,y,t)|\uparrow\rangle \tag{34}$$

$$= \frac{\sigma_{\uparrow\uparrow}}{N(t)}\int_0^\infty |g_\uparrow(y,t)|^2\, dy. \tag{35}$$

The yield $N(t)$ can be calculated without explicit knowledge of $g_\downarrow$, since the Gaussian solutions are related by reflection symmetry: $g_\uparrow(y,t)=g_\downarrow(-y,t)$. We choose various magnetic field gradients ranging from 0.1 to 100 T $\mu$m$^{-1}$ and plot the output fidelity of a maximally mixed input state as a function of the Q1DC angle $\theta$ and the gate time $t$ (see Fig. 7). Perfect spin filtering corresponds to a fidelity $F=1$, and the worst-case fidelity is $F=\frac{1}{2}$. The density plots show how the optimal parameter regions increase with larger magnetic field gradients. This model is useful in determining the appropriate gate geometry and field gradients required to achieve good fidelities.

The technology of nanoscale single domain magnets is not yet capable of producing large fields in arbitrary configurations. The above linearly inhomogeneous magnetic field is therefore a simple approximation to the real magnetic field configuration on any particular device. In the next subsection we consider the effect of a different (perhaps more realistic) field configuration, namely, the field near one of the poles of a dipole magnet.

### C. Stern–Gerlach gate with dipole field

In this subsection we study the quality of the readout obtained from a Stern–Gerlach type gate driven by a simple 2D dipole field lying in the 2DEG plane, as shown in Fig. 8. In the Appendix, we derive the magnetic vector potential

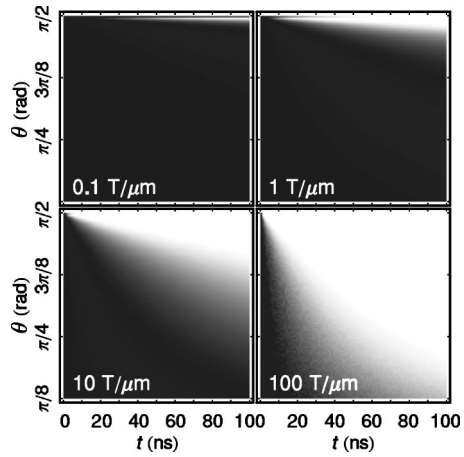


FIG. 7. Fidelity $F_{\uparrow}$ in the $C_{\uparrow}$ channel for a Stern–Gerlach gate operated by a linearly inhomogeneous and unidirectional magnetic field in the $y$ direction. White regions$\Rightarrow F_{\uparrow}=1$. $\theta$ is the angle between the Q1DC and SAW direction. $t$ is the gate time. Input state is a maximally mixed spin state in the groundstate of the SAW quantum dot. Various magnetic field gradients have been chosen to show the increase in the optimal parameter region (white) in the $(t,\theta)$ plane with increasing field gradient. $t_{\max}\approx 100$ ns is a crude order of magnitude estimate for the GaAs spin relaxation lifetime.

$$A_z = \frac{\beta x}{x^2 + (y-d)^2}, \tag{36}$$

where $\beta$ is a strength parameter and $d$ is the distance of the 2D dipole from the Q1DC.

Figure 8 shows that the gradient of the field in the $y$ direction reverses direction at two points, $x=\pm d$. In order to prevent the moving qubit from experiencing opposite field gradients, we will restrict the gate time to $T=2d$ so that the qubit moves in the region $-T/2<x<T/2$ in the laboratory frame. The question of how we are to shield the extraneous field from the qubit does not have a simple solution. It has been suggested that a superconducting material such as Niobium could be used to shield the magnetic field where it is not needed.[5]

The results of a 1D simulation of the wavefunction along the $x=z=0$ direction are shown in Fig. 9. The numerical method used was a Crank–Nicholson algorithm adapted to the Pauli equation. The plot shows three time-shots of the probability density $|\psi(y)^2|$, normalized to peak. The initial

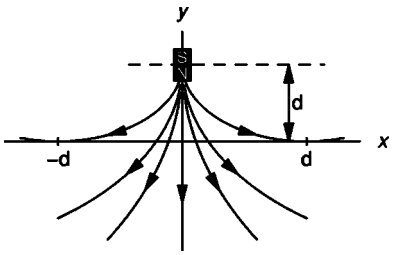


FIG. 8. Vector field plot in the $xy$ (2DEG) plane showing the magnetic field due to an infinite string of dipole moments running parallel to the $z$ axis at a distance $d$ from the Q1DC.

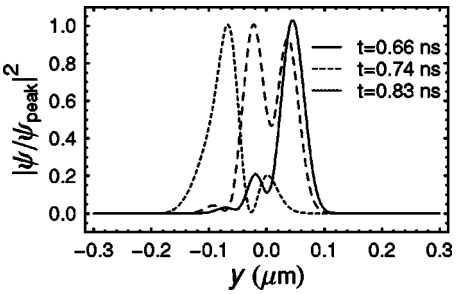


FIG. 9. Three time-shots (see legend) showing the spatial electron probability density (normalized to peak). $y$ is the direction transverse to the Q1DC. This is a Stern–Gerlach type readout gate using the 2D dipole field (1 T$\mu$m$^{-1}$ at $x=y=0$) shown in Fig. 8. Initial condition is a Gaussian wavepacket with spin $|\uparrow_y\rangle$. Sideways translation of the probability density is suppressed due to both the strongly confining effective potential arising from the $A^2$ term and the precessional motion of the Bloch vector in the non-unidirectional field.

state is a Gaussian groundstate with spin state $|\uparrow_y\rangle$. The simulation shows no significant spatial displacement of the electron density in the $y$ directions, in contrast to the behavior exhibited under the linearly inhomogeneous field [cf. Eq. (26)]. This is partially due to the effect of the Lorentz force generated by the $A^2$ term in the Hamiltonian, which contributes an effective potential that is highly confining in the $y$ direction. The $A^2$ confinement is so strong that the Q1DC opening angle $\theta$ becomes irrelevant. Bohr and Pauli's claim that the Lorentz force washes out the Stern–Gerlach effect is upheld in this particular scenario.

Another source of problems for this field configuration is that the $|\uparrow_y\rangle$, $|\downarrow_y\rangle$ states are not eigenstates of the field as they were with the linearly inhomogeneous field. Figure 10 shows the evolution of the Bloch vector in a spin-only model of the electron spin qubit. It demonstrates how the Bloch vector begins precessing about the $x$ component of the magnetic field, causing the Stern–Gerlach force to act in different directions. Although careful timing of the gate and possible compensation mechanisms could be put in place, this gate is essentially not robust. We draw the conclusion that in param-

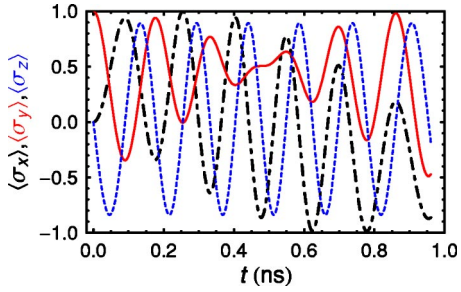


FIG. 10. (Color online) Evolution of the Bloch vector in a 2D dipole field (1 T$\mu$m$^{-1}$ at $x=y=0$): $\langle\sigma_x\rangle$ (long-short dash), $\langle\sigma_y\rangle$ (solid), $\langle\sigma_z\rangle$ (short dash). Time $t=0$ corresponds to the starting point $x=-d$ (see Fig. 8). We have used a spin-only model of the electron spin qubit to illustrate spin precession in the non-unidirectional field. The Bloch vector changes direction rapidly, which in turn causes the Stern–Gerlach force to fluctuate during the operation of the gate.

eter regimes relevant to single-electron transport by SAW in GaAs, a field of this type will not be suitable for a Stern–Gerlach measurement gate, and that field unidirectionality is generally an important requirement for quantum gates driven by static magnetic fields.

## V. DECOHERENCE EFFECTS

The major effects of decoherence on this SAW quantum computing system have already been considered qualitatively in the original proposal and subsequent papers,[5,31] and more specifically by a number of authors. These effects include the following: The interaction of the electron qubit with other electrons in the 2DEG, surface gates, and donor impurities,[31,59] the coupling of qubits to phonons,[60,61] nuclear spins[7] and radio-frequency photons.[62]

The models we have presented here give rise to behavior which was previously neglected in the original proposal for the quantum computation scheme.[5] They allow us to predict the contribution to decoherence from excitation into higher orbital states and give their probabilities of occupation.

Any potential decoherence due to tunneling between neighboring dots is negligible, and if needed the spatial separation of qubits can be increased by either introducing higher harmonics of the SAW fundamental frequency or by active gating at the entrance to each Q1DC. A major source of error is the current fluctuations in the quantized single-electron SAW current. In recent experiments,[32,33] errors in the current quantization (including shot and Johnson noise) of less than 0.1% were observed.

The relevant decoherence timescales that underpin our proposals is the spin lifetime ($T_1$ and $T_2$) of single electrons in quantum dots. For *n*-type bulk semiconductors, $T_1$ spin lifetimes in GaAs of 100 ns have been reported, which gives a very crude ball-park figure.[63] An estimate that is more relevant to the SAW electron system is the spin relaxation lifetime of a few nanoseconds, which was obtained from spin-resolved microphotoluminescence spectroscopy measurements on photoexcited electrons.[64] However, this is the worst-case scenario because the method of electron capture we propose[5] produces a conduction-band hole that is more extended, short-lived and mixed than the photoexcited hole. Indeed, recent experiments on static GaAs quantum dots report a lower bound on $T_1$ as long as 50 $\mu$s,[65] which makes an estimate of 100 ns for the $T_1$ lifetime of SAW electrons quite reasonable in the light of current technology.

## VI. SUMMARY

We have analyzed in detail a proposal[5] for implementing quantum computation on electron spin qubits trapped in SAW-Q1DC electrostatically defined dots, using only static magnetic gates to perform single-qubit initializations, rotations and readouts. Applying the full Pauli Hamiltonian, we described the quantum dynamics of both the spin and orbital states of the qubit for various parameter regimes relevant in SAW single-electron transport experiments. In the analysis of single-qubit unitary operations with localized uniform magnetic fields, we showed that the effect of the Lorentz force puts limits on field strengths and gate times. Moreover, simulations showed that field directions normal to the 2DEG excite rotational states in the dot. Probabilities of excitation into higher-energy orbitals were given. In terms of feasibility, the models indicate that a field strength of about 80 mT will be sufficient to conduct a $\pi$ rotation in about 1 ns, without compromising the confinement properties of the trapped qubit. Since $T_1$ spin lifetimes of microseconds have been reported,[65] it is feasible for hundreds of single-qubit gates to operate before all coherence is lost in the computation.

We also studied a device for single-qubit measurement and initialization based on the Stern–Gerlach effect. The problematic Lorentz force can be partly suppressed by virtue of the geometry of the 2DEG system, and for a unidirectional, linearly inhomogeneous field, the correlation between the spin states and spatial location of the qubit leads to a good quantum measurement of its spin. For a 2D dipole field, the vector potential has a deleterious effect. Namely, it contributes an effective confining potential via the $A^2$ term in the Pauli Hamiltonian which suppresses the transverse motion in the *y* direction. Furthermore, the component of magnetic field in the *x* direction causes the Bloch vector to rotate in undesired directions. The latter problem could be overcome by using unitary gates prior to the Stern–Gerlach gate to correct any spurious rotations, but it is unlikely that such a finely tuned arrangement can be made robust. Magnetic fields that are good approximations to a unidirectional and linearly inhomogeneous field can provide a source of polarized electron qubit states in channels $C_\uparrow$ and $C_\downarrow$ with high yield. The very same gate can be used to measure the ratio $|\alpha|^2/|\beta|^2$ for an input qubit state $|\psi\rangle = \alpha|\uparrow_y\rangle + \beta|\downarrow_y\rangle$. The advantages of this readout method are that the averaging time of the measured current can be made long enough to render most noise sources (e.g., shot noise, input-referred noise of the current pre-amp) unimportant, and that missing electrons from SAW minima do not contribute any error since we are measuring the ratio of currents out of the two channels. Field gradients in the range $0.1-100\ \mathrm{T}\mu\mathrm{m}^{-1}$ lead to gate times that are easily within the range of $T_1$ spin lifetimes in GaAs. These parameter regimes will need to be probed by experiment if we are to make progress towards feasible quantum computation with nanomagnets in the SAW quantum computer.

## ACKNOWLEDGMENTS

The authors would like to thank Sean Barrett, Masaya Kataoka, Alexander Moroz, Andy Robinson and Tom Stace for their ideas and helpful discussions. The authors gratefully acknowledge the support of the EPSRC. This work was partly funded by the Cambridge–MIT institute.

## APPENDIX: DERIVATION OF THE 2D DIPOLE FIELD VECTOR POTENTIAL

We adopt cylindrical coordinates $(r, \phi, y)$ about the *y* axis, with $r = \sqrt{x^2 + z^2}$. We consider the field due to an infinite string of dipoles passing parallel to the *z* axis through $y = d$ as

shown in Fig. 8. The resulting magnetic field has planar symmetry with respect to the *xy* (2DEG) plane. The Q1DC runs along the *x* axis. A vector potential for this field can be constructed as follows. A magnetic dipole at $y=z=0$ pointing in the $+y$ direction has a vector potential[66]

$$A'_\phi(r,y) = \frac{\mu_0 m_B dz}{4\pi} \frac{r}{(r^2+y^2)^{3/2}}, \tag{A1}$$

where $A'_r = A'_y = 0$ and $m_B$ is the dipole moment per unit length in the $z$ direction. We now displace this potential by $d$ in the $y$ direction and integrate over all $z$, obtaining

$$A_z = \frac{\beta x}{x^2 + (y-d)^2}, \tag{A2}$$

with $A_x = A_y = 0$ and strength parameter $\beta = \mu_0 m'_B / 2\pi$. The magnetic field can be derived by applying the curl in cylindrical coordinates: $B_r = -r^{-1}\partial_y(rA_\phi)$ and $B_y = r^{-1}\partial_r(rA_\phi)$. Figure 8 shows the vector field plot of the resulting magnetic field, which falls off as $r^{-2}$ for large $r$.

*Also affiliated with Centre for Quantum Computation, Department of Applied Mathematics and Theoretical Physics, Wilberforce Road, Cambridge CB3 0WA, UK. Electronic address: suguru.furuta@qubit.org

[1] R. Feynman, Int. J. Theor. Phys. **21**, 467 (1982).
[2] P. Shor, in *Proceedings of 35th Annual Symposium on Foundations of Computer Science* (1994), pp. 124–134, quant-ph/9508027.
[3] A. Ekert and R. Jozsa, Rev. Mod. Phys. **68**, 733 (1996).
[4] M. Nielson and I. Chuang, *Quantum Computation and Quantum Information* (Cambridge U.P., Cambridge, 2000).
[5] C. H. W. Barnes, J. M. Shilton, and A. M. Robinson, Phys. Rev. B **62**, 8410 (2000).
[6] D. Loss and D. P. DiVincenzo, Phys. Rev. A **57**, 120 (1998).
[7] G. Burkard, D. Loss, and D. P. DiVincenzo, Phys. Rev. B **59**, 2070 (1999).
[8] D. Loss, G. Burkard, and E. Sukhorukov, in *Proceedings of the XXXIVth Rencontres de Moriond* "Quantum Physics at Mesoscopic Scale" (1999), cond-mat/9907133.
[9] F. Troiani, U. Hohenester, and E. Molinari, Phys. Rev. B **62**, R2263 (2000).
[10] D. P. DiVincenzo, D. Bacon, J. Kempe, G. Burkard, and K. B. Whaley, Nature (London) **408**, 339 (2000).
[11] J. M. Elzerman, R. Hanson, J. S. Greidanus, L. H. Willems van Beveren, S. D. Franceschi, L. M. K. Vandersypen, S. Tarucha, and L. P. Kouwenhoven, Phys. Rev. B **67**, 161308(R) (2003).
[12] T. Calarco, A. Datta, P. Fedichev, E. Pazy, and P. Zoller, Phys. Rev. A **68**, 012310 (2003).
[13] J. M. Shilton, V. I. Talyanskii, M. Pepper, D. A. Ritchie, J. E. F. Frost, C. J. B. Ford, C. G. Smith, and G. A. C. Jones, J. Phys.: Condens. Matter **8**, L531 (1996).
[14] V. I. Talyanskii, J. M. Shilton, M. Pepper, C. G. Smith, C. J. B. Ford, E. H. Linfield, D. A. Ritchie, and G. A. C. Jones, Phys. Rev. B **56**, 15180 (1997).
[15] V. I. Talyanskii, J. M. Shilton, J. Cunningham, M. Pepper, C. J. B. Ford, C. G. Smith, E. H. Linfield, D. A. Ritchie, and G. A. C. Jones, Physica B **251**, 140 (1998).
[16] R. Vrijen, E. Yablonovitch, K. Wang, H. W. Jiang, A. Balandin, V. Roychowdhury, T. Mor, and D. DiVincenzo, Phys. Rev. A **62**, 012306 (2000).
[17] B. E. Kane, Nature (London) **393**, 133 (1998).
[18] Y. Makhlin, G. Schon, and A. Shnirman, Rev. Mod. Phys. **73**, 357 (2001).
[19] D. J. Wineland, M. Barrett, J. Britton, J. Chiaverini, B. L. DeMarco, W. M. Itano, B. M. Jelenkovic, C. Langer, D. Leibfried, V. Meyer *et al.*, Philos. Trans. R. Soc. London, Ser. A **361**, 1349 (2003).
[20] E. Knill, L. Laflamme, and G. J. Milburn, Nature (London) **409**, 46 (2001).
[21] J. I. Cirac and P. Zoller, Nature (London) **404**, 579 (2000).
[22] A. Bertoni, P. Bordone, R. Brunetti, C. Jacoboni, and S. Reggiani, Phys. Rev. Lett. **84**, 5912 (1999).
[23] A. E. Popescu and R. Ionicioiu, Phys. Rev. B **69**, 245422 (2004).
[24] I. L. Chuang, N. Gershenfeld, M. G. Kubinec, and D. W. Leung, Proc. R. Soc. London, Ser. A **454**, 447 (1998).
[25] D. G. Cory, A. F. Fahmy, and T. F. Havel, Proc. Natl. Acad. Sci. U.S.A. **94**, 1634 (1997).
[26] J. A. Jones, Philos. Trans. R. Soc. London, Ser. A **361**, 1429 (2003).
[27] R. Ionicioiu, P. Zanardi, and F. Rossi, Phys. Rev. A **63**, 050101(R) (2001).
[28] M. Kitagawa and M. Ueda, Phys. Rev. Lett. **67**, 1852 (1991).
[29] M. J. Kelly, *Low-Dimensional Semiconductors: Materials, Physics, Technology, Devices* (Clarendon, Oxford, 1995).
[30] P. Utko, K. Gloos, J. B. Hansen, and P. E. Lindelof, Acta Phys. Pol. A **103**, 533 (2003).
[31] A. M. Robinson and C. H. W. Barnes, Phys. Rev. B **63**, 165418 (2001).
[32] A. M. Robinson, V. I. Talyanskii, M. Pepper, J. E. Cunningham, E. H. Linfield, and D. A. Ritchie, in Inst. Phys. Conf. Ser. (2003), Vol. 171.
[33] A. M. Robinson, V. I. Talyanskii, M. Pepper, J. E. Cunningham, E. H. Linfield, and D. A. Ritchie, Phys. Rev. B **65**, 045313 (2002).
[34] W. M. Kaminsky, G. A. C. Jones, N. K. Patel, W. E. Booij, M. G. Blamire, S. M. Gardiner, Y. B. Xu, and J. A. C. Bland, Appl. Phys. Lett. **78**, 1589 (2001).
[35] R. Nemutudi, C. G. Smith, C. J. B. Ford, N. J. Appleyard, M. Pepper, D. A. Ritchie, and G. A. C. Jones, J. Vac. Sci. Technol. B **20**, 2810 (2002).
[36] R. Nemutudi, N. J. Curson, N. J. Appleyard, D. A. Ritchie, and G. A. C. Jones, Microelectron. Eng. **57-8**, 967 (2001).
[37] N. J. Curson, R. Nemutudi, N. J. Appleyard, M. Pepper, D. A. Ritchie, and G. Jones, Appl. Phys. Lett. **78**, 3466 (2001).
[38] J. Crank and P. Nicolson, in Proc. Cambridge Philos. Soc. (1947), Vol. 32, p. 50.
[39] S. Datta and B. Das, Appl. Phys. Lett. **56**, 665 (1990).
[40] Y. Ohno, D. K. Young, B. Beschoten, F. Matsukura, H. Ohno, and D. D. Awschalom, Nature (London) **402**, 790 (1999).
[41] R. Ionicioiu and I. D'Amico, Phys. Rev. B **67**, 041307(R) (2003).

[42] C. I. Pakes, V. Conrad, J. C. Ang, F. Green, A. S. Dzurak, L. C. L. Hollenberg, D. N. Jamieson, and R. G. Clark, Nanotechnology **14**, 161 (2003).
[43] M. Friesen, C. Tahan, R. Joynt, and M. A. Eriksson, Phys. Rev. Lett. **92**, 037901 (2004).
[44] T. M. Stace and S. D. Barrett, Phys. Rev. Lett. **92**, 136802 (2004).
[45] H.-S. Goan and G. J. Milburn, Phys. Rev. B **64**, 235307 (2001).
[46] A. N. Korotkov, Phys. Rev. B **63**, 085312 (2001).
[47] W. Gerlach and O. Stern, Z. Phys. **9**, 349 (1922).
[48] A. Challinor, A. Lasenby, S. Gull, and C. Doran, Phys. Lett. A **218**, 128 (1996).
[49] A. Venugopalan, D. Kumar, and R. Ghosh, Physica A **220**, 576 (1995).
[50] N. F. Mott and H. S. W. Massey, *The Theory of Atomic Collisions* (Oxford University Press, Oxford, 1965), Chap. IX.1.
[51] W. Pauli, in *Proceedings of the Sixth Solvay Conference* (Gauthier-Villars, Brussels, 1932), pp. 183–186.
[52] H. Batelaan, T. J. Gay, and J. J. Schwendiman, Phys. Rev. Lett. **79**, 4517 (1997).
[53] B. M. Garraway and S. Stenholm, Phys. Rev. A **60**, 63 (1999).
[54] G. A. Gallup, H. Batelaan, and T. J. Gay, Phys. Rev. Lett. **86**, 4508 (2001).
[55] H. Dehmelt, Science **247**, 539 (1990).
[56] J. Fabian and S. Das Sarma, Phys. Rev. B **66**, 024436 (2002).
[57] A. Peres, *Quantum Theory: Concepts and Methods* (Kluwer, Dordrecht, 1993).
[58] R. Crook, A. C. Graham, C. G. Smith, I. Farrer, H. E. Beere, and D. A. Ritchie, Nature (London) **424**, 751 (2003).
[59] S. D. Barrett and G. J. Milburn, Phys. Rev. B **68**, 155307 (2003).
[60] V. N. Golovach, A. Khaetskii, and D. Loss, Phys. Rev. Lett. **93**, 016601 (2004).
[61] Y. G. Semenov and K. W. Kim, Phys. Rev. Lett. **92**, 026601 (2004).
[62] Y. Yamamoto and A. Imamoglu, *Mesoscopic Quantum Optics* (Wiley, New York, 1999).
[63] J. M. Kikkawa and D. D. Awschalom, Phys. Rev. Lett. **80**, 4313 (1998).
[64] T. Sogawa, P. V. Santos, S. K. Zhang, S. Eshlaghi, A. D. Wieck, and K. H. Ploog, Phys. Rev. Lett. **87**, 276601 (2001).
[65] R. Hanson, B. Witkamp, L. M. K. Vandersypen, L. H. Willems van Beveren, J. M. Elzerman, and L. P. Kouwenhoven, Phys. Rev. Lett. **91**, 196802 (2003).
[66] J. D. Jackson, *Classical Electrodynamics*, 2nd ed. (Wiley, New York, 1975), p. 194.
[67] In other words, we ignore the $z$ dependence of the wavefunction. This is partly justified if $e\beta\Delta x/\sqrt{\Delta E m^*} \ll 1$, where $\Delta E$ is the characteristic energy gap between the 2DEG energy bands and $\Delta x$is the length of the gate. This is indeed the case for parameter regimes that we consider.
[68] The spreading time for a Gaussian state is the time taken for its standard deviation to double.